Influence of crystal field on anisotropic x-ray magnetic linear dichroism at the Co²⁺ $L_{2,3}$ edges

Gerrit van der Laan[*]

Diamond Light Source, Chilton, Didcot, Oxfordshire OX11 0DE, United Kingdom
and Magnetic Spectroscopy Group, Daresbury Laboratory, Warrington WA4 4AD, United Kingdom

Elke Arenholz

Advanced Light Source, Lawrence Berkeley National Laboratory, Berkeley, California 94720, USA

Rajesh V. Chopdekar[†] and Yuri Suzuki

Department of Materials Science and Engineering, University of California–Berkeley, Berkeley, California 94720, USA

We expand the previous theoretical treatment for the strong anisotropy of the x-ray magnetic linear dichroism (XMLD) in a crystal field of cubic point-group symmetry to the more general case of tetragonal point-group symmetry. For the cubic symmetry, there are only two fundamental spectra, which have the same shape for rotation of either linear light polarization **E** or magnetization direction **H**. For the tetragonal symmetry, the XMLD is a linear combination of four fundamental spectra, with a different shape for linear dichroism (rotation of **E**) and magnetic dichroism (rotation of **H**). However, only one extra spectrum is required to relate the linear and magnetic dichroism. The validity of the theory is demonstrated using a CoFe₂O₄(011) thin film on SrTiO₃, which has both tetrahedrally distorted symmetry and large magnetic anisotropy. The XMLD at the Co $L_{2,3}$ edges was found to exhibit a strong dependence on the relative orientation of external magnetic field, x-ray polarization, and crystalline axes. The large variations in the peak structure as a function of angle are not caused by the spin-orbit-induced magnetocrystalline anisotropy but arise from the symmetry of the measurement geometry. The results are compared with calculated spectra using atomic multiplet theory for Co²⁺ d^7 → $2p^5 d^8$ in octahedral and tetragonal crystal field symmetry. Although the magnitude of the dichroism is strongly influenced by the temperature, its spectral shape remains largely unaffected. The measured fundamental spectra are also robust against incomplete magnetization. The influence of the tetragonal distortion is revealed by small differences between the linear and magnetic dichroism. It is shown that the magnetic dichroism spectra can be transferred from CoFe₂O₄ to CoO. Therefore, the rich structure in the Co²⁺ L_3 XMLD provides a sensitive probe to determine the orientation of the spin axis with respect to the crystalline axes, hence offering a valuable tool for experimentalists for the study of exchange bias in Co oxides. In contrast, the Co²⁺ L_2 edge, where the fundamental spectra have similar spectral shape but with opposite sign, does not allow an unambiguous determination.

I. INTRODUCTION

Magnetic moments in antiferromagnetic materials are arranged in two sublattices that compensate each other perfectly. They hence have no macroscopic magnetization and are not sensitive to moderate external magnetic fields. This provides the ability to fix or "pin" the orientation of a ferromagnetic film by exchange coupling to an antiferromagnet,[1,2] which has found widespread use in magnetic data-recording devices. However, the vanishing magnetization also renders antiferromagnets a difficult class of materials to study, not accessible to element-specific probes such as x-ray magnetic circular dichroism (XMCD). Soft x-ray magnetic linear dichroism (XMLD) has been developing into a powerful tool to study the magnetic order in antiferromagnetic materials down to the microscopic level.[3] In a typical XMLD experiment, the difference in x-ray absorption (XA) of linearly polarized x rays with parallel and perpendicular orientation of light polarization and magnetization axis is determined. XMLD is sensitive to uniaxial magnetic order, so that ferri- and antiferromagnetic materials as well as ferromagnetic systems can be probed.[4,5] Using the sum rules,[6,7] XMLD also offers the possibility to determine the anisotropy of the spin-

orbit interaction, which is proportional to the magnetocrystalline anisotropy energy.

Until recently, it was commonly assumed that the spectral shape and magnitude of the XMLD signal are solely determined by the relative orientation of magnetic moments and polarization vector of the light. In studies in the literature it is common to find that the orientation of moments and polarization relative to the crystal lattice is not specified unambiguously, e.g., while the angle to the surface normal is noted, the in-plane angle is not.[8,9] Recently, however, it has been observed that a change of the relative orientation of spin axis and x-ray polarization with respect to the crystallographic directions leads to large differences in the XMLD spectrum[10–14]—and in some cases even to a complete reversal of this spectrum. The measured anisotropy in the XMLD of localized systems obeys the angular dependence of the lattice[11] and has been successfully described using multiplet calculations for the Mn $L_{2,3}$ edges in (Mn,Ga)As,[10] Fe $L_{2,3}$ edges in Fe₃O₄,[11] and Ni $L_{2,3}$ edges in NiO and NiFe₂O₄.[12]

Besides the above mentioned near-cubic systems, other more complicated systems would strongly benefit if they could be studied by anisotropic XMLD. Compared to Fe and Ni oxides, the large magnetic anisotropy and tendency for

tetragonal distortion of Co oxides provide additional challenges in the study of XMLD. Therefore, in order to investigate these systems, it is necessary to generalize previous results obtained for cubic symmetry. The extension to lower symmetry, which is the subject of this paper, not only allows us to obtain a satisfactory description for Co^{2+}, but also provides deeper insight into the origin of the anisotropic XMLD.

Ferrimagnetic $CoFe_2O_4$ is attractive for magnetic recording applications, and has been successfully integrated as the pinning layer in spin valve structures and spin filters with large magnetoresistance.[15–18] The Co spinel exhibits a high magnetocrystalline anisotropy and a large magnetostriction.[19–23] Recent band-structure calculations also suggested a half-metallic character.[24]

CoO is a rocksalt antiferromagnetic insulator with a Néel temperature of ~ 291 K,[25] below which it undergoes a tetragonal contraction. CoO has a large orbital magnetic moment and spin-orbit coupling,[26] so there is a strong coupling between spin and lattice, giving rise to a large magnetic anisotropy. Thin films and granular layers of CoO are widely used as antiferromagnets for exchange bias.[27–33] Brillouin light scattering showed that the magnetic anisotropy is related to the crystallographic symmetry of the ferromagnetic and antiferromagnetic layers.[34]

None of the spintronics results may be properly understood without knowing beforehand the structural, chemical, and magnetic properties of the materials involved. The intense current interest in the magnetic properties of $CoFe_2O_4$ and CoO indicates that a thorough analysis and detailed theoretical understanding of the Co^{2+} XMLD is timely and essential. We will show how the XMLD at the Co $L_{2,3}$ edges can be used as a powerful tool to determine the orientation of the spin axis in $CoFe_2O_4$ and CoO. The big advantage of studying the ferrimagnet $CoFe_2O_4$, instead of the antiferromagnet CoO, is that in the ferrimagnet the magnetization direction can be manipulated using an external magnetic field, allowing clear separation of the magnetic and nonmagnetic contributions to the XMLD signal.[6]

The outline of this paper is as follows. Experimental details are described in Sec. II. General expressions for the XMLD are presented in Sec. III, describing its angular dependence in tetragonal and cubic crystal field symmetry, and discussing the difference between rotation of the light polarization (i.e., linear dichroism) and the magnetization direction (i.e., magnetic dichroism), the relation to the magnetic anisotropy, and the effect of nonsaturated magnetization. The calculation of the fundamental spectra for the Co^{2+} $L_{2,3}$ edges is treated in Sec. IV, together with the temperature dependence of the dichroism. Practical and wider applications and the way to determine the direction of the spin axis are discussed in Sec. V. Conclusions are drawn in Sec. VI.

II. EXPERIMENT

Epitaxial $CoFe_2O_4$ films, 40 nm thick, were deposited on $SrTiO_3(011)$ single substrates by pulsed laser deposition at 450 °C in 10^{-6} Torr vacuum. $CoFe_2O_4$ ($a=8.36$ Å) is under compressive strain from the substrate ($a=3.91$ Å). Strain ef-

fects combined with the magnetocrystalline contribution to the magnetic anisotropy give rise to an easy [100] and hard [01$\bar{1}$] direction in these films.[35] Our films exhibit good crystallinity as observed by x-ray diffraction and Rutherford backscattering spectroscopy.

The XMLD experiments were performed on beamline 4.0.2 at the Advanced Light Source,[36] providing linearly polarized x rays with polarization direction continuously tunable through a 90° range and a degree of polarization of $(99 \pm 1)\%$. The eight-pole resistive magnet employed for these experiments allows applying magnetic fields up to 0.8 T in any direction.[37] All spectra were obtained by monitoring the sample drain current, i.e., in electron-yield mode, in normal incidence at $T=420$ K in external fields of 0.55 T. At lower temperatures the available external fields are not sufficient to align the Co moments even along the easy magnetization direction [100]. In order to increase the electron-yield signal, the magnetic field was turned slightly out of the sample surface plane. Since this is a hard magnetic axis for the $CoFe_2O_4$ thin film, this barely influences the orientation of the magnetic moments.

The Co $L_{2,3}$ XA, XMCD, and XMLD spectra measured for $CoFe_2O_4/SrTiO_3(011)$ are plotted in Fig. 1. The measured XA and XMCD are in good agreement with previously reported results.[38,39] The spectral shape of the XMCD did not show a conspicuous angular dependence, in accordance with earlier measurements of $3d$ transition metals in cubic symmetry.[40] On the other hand, the experimental XMLD spectra, I_0, I_{45}, and $I_{90}^{\theta=45}$, i.e., the XMLD spectra measured for $\phi=0°$, 45°, and 90° [the precise definition is supplied by Eq. (1b) of Sec. III], show huge changes in the spectral shape.

III. THEORY

A. Definition of the geometry

Since there are many different ways to choose the geometry of the XMLD experiment, this concept requires a detailed and precise description. We also need to make a convenient choice of coordinate system in order to be able to write down concise analytical expressions.

Taking an orthogonal coordinate system along the crystal axes $x\|[010]$, $y\|[001]$, and $z\|[100]$, we define a spherical polar coordinate system with the polar axis along z. An arbitrary direction has a polar angle ϕ with respect to the $z\|[100]$ axis and azimuthal angle θ with respect to the zx plane [$=(001)$ plane]; see Fig. 2 for a schematic drawing.

The underlying idea is that θ defines the *plane of orientation*, which contains both the linear polarization direction **E** of the x rays and the magnetization direction **H** of the applied field [cf. Eq. (1) below]. Hence θ is a fixed angle for a given measurement plane, e.g., $\theta=0°$ and 45° correspond to the (001) and (01$\bar{1}$) planes, respectively. For practical experimental reasons the plane of orientation will normally be parallel to the sample surface plane, as is the case in this paper.

Regarding the notation, the angle ϕ is here defined in the same way as in Ref. 10. In Ref. 11 we used ϕ_S, but we omit
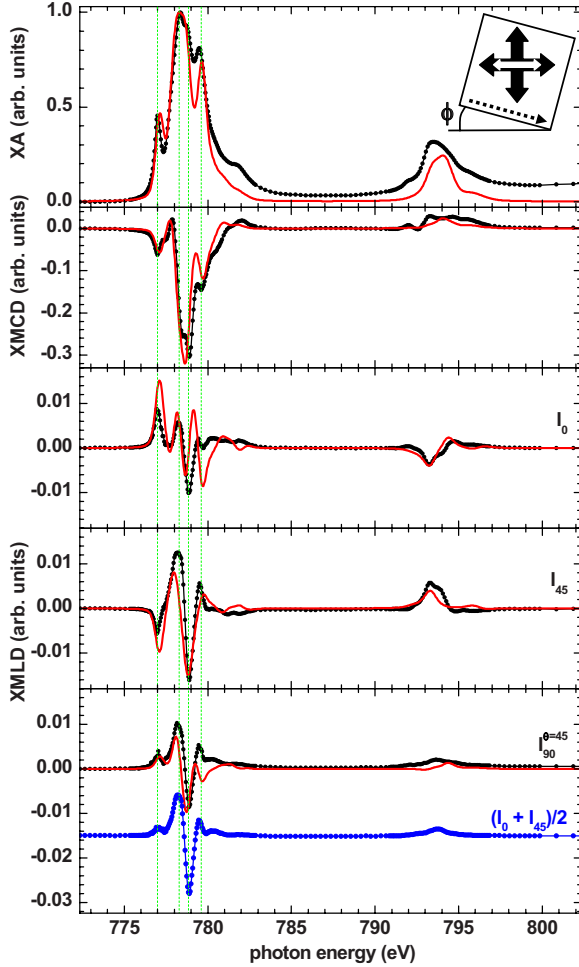
FIG. 1. (Color online) Co $L_{2,3}$ XA, XMCD, and XMLD spectra (I_0, I_{45}, and $I_{90}^{\theta=45}$) measured from CoFe$_2$O$_4$/SrTiO$_3$(011). Experimental spectra (black dots) obtained at $T=420$ K and $H=0.55$ T. Calculated spectra (red curves), also shown in Fig. 4. The intensities are on an arbitrary scale. The mean spectrum $(I_0+I_{45})/2$ (blue dots) obtained from the measured I_0 and I_{45} spectra is shown for comparison to the $I_{90}^{\theta=45}$ spectrum. The thin dashed vertical lines (green) are an aid to compare the various features in the L_3 edge across the different spectra. The inset depicts the experimental geometry. The linear polarization of the x rays (white double-headed arrow) makes an angle ϕ with the [100] axis (dashed arrow) of the sample. The XMLD is the difference spectrum between two perpendicular orientations of the external magnetic field (black double-headed arrows), i.e., $I_\phi=I_{XA}(\mathbf{E}_\phi,\mathbf{H}_\phi)-I_{XA}(\mathbf{E}_\phi,\mathbf{H}_{\phi+90°})$ in the (011) surface plane.

here the subscript S, indicating the sample rotation, which is redundant since we do not treat any other geometry than what is called geometry 3 in Ref. 11. In contrast to Ref. 11 we specify the plane of orientation by the angle θ, instead of the lattice indices. This has the advantage that the geometric part of the expression for the XMLD contains only angular variables, making the formulas easy to handle.

The XMLD is the difference between two XA spectra measured with different orientations of $\mathbf{H}$ and $\mathbf{E}$ in the plane of orientation. Either $\mathbf{E}$ or $\mathbf{H}$ is rotated by (preferably) 90° between the two successive XA measurements, leading to
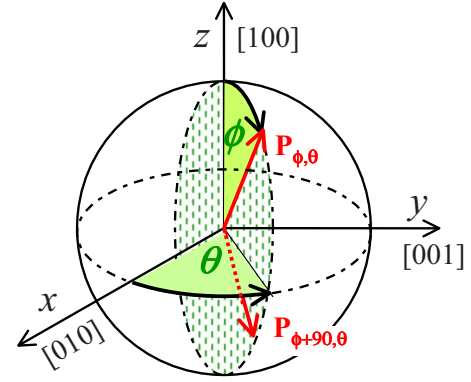

FIG. 2. (Color online) Definition of the measurement geometry. In the right-handed orthogonal coordinate frame of the crystal with $x\|[010]$, $y\|[001]$, and $z\|[100]$, we define a spherical polar coordinate system with the polar axis along z. A vector $\mathbf{P}_{\phi,\theta}$ [red (gray) solid arrow] has polar angle ϕ with respect to the z axis and azimuthal angle θ with respect to the (001) plane (=zx plane). Also drawn is a vector $\mathbf{P}_{\phi+90°,\theta}$ [red (gray) dotted arrow]. These two vectors define a plane of orientation (vertically dashed plane) with fixed azimuthal angle θ, e.g., $\theta=0°$ and 45° correspond to the (001) and (01$\bar{1}$) planes, respectively. The linear dichroism (LD) is obtained by rotating $\mathbf{E}$ as $I_{LD}(\phi,\theta)=I_{XA}(\mathbf{E}_{\phi,\theta},\mathbf{H}_{\phi,\theta})-I_{XA}(\mathbf{E}_{\phi+90,\theta},\mathbf{H}_{\phi,\theta})$. The magnetic dichroism (MD) is obtained by rotating $\mathbf{H}$ as $I_{MD}(\phi,\theta)=I_{XA}(\mathbf{E}_{\phi,\theta},\mathbf{H}_{\phi,\theta})-I_{XA}(\mathbf{E}_{\phi,\theta},\mathbf{H}_{\phi+90,\theta})$.

either linear dichroism (LD) or magnetic dichroism (MD), respectively,

$$I_{LD}(\phi,\theta) = I_{XA}(\mathbf{E}_{\phi,\theta},\mathbf{H}_{\phi,\theta}) - I_{XA}(\mathbf{E}_{\phi+90,\theta},\mathbf{H}_{\phi,\theta}), \quad (1a)$$

$$I_{MD}(\phi,\theta) = I_{XA}(\mathbf{E}_{\phi,\theta},\mathbf{H}_{\phi,\theta}) - I_{XA}(\mathbf{E}_{\phi,\theta},\mathbf{H}_{\phi+90,\theta}), \quad (1b)$$

where the indices refer to the polar and azimuthal angles. For the measurements shown in Fig. 1, the XMLD signal is obtained as in Eq. (1b). For each different XMLD spectrum in this geometry (see inset to Fig. 1) the sample is rotated to an angle ϕ (between $\mathbf{E}$ and [100]) about the surface normal, [011], which corresponds to a plane of measurement with $\theta=45°$. The XMLD is then the difference of the XA spectra measured with $\mathbf{H}$ parallel and perpendicular to $\mathbf{E}$, respectively.

Finally, we note that $\mathbf{E}$ and $\mathbf{H}$ act in the case of XMLD as axial vectors, which are invariant for inversion, i.e., $\mathbf{P}_{\phi,\theta}=\mathbf{P}_{180-\phi,\theta+180}$. Also, when zx is a mirror plane of the crystal we have $\mathbf{P}_{\phi,\theta}=\mathbf{P}_{\phi,-\theta}$ and active and passive rotations over θ give the same result, so that the (011) and (01$\bar{1}$) planes are equivalent.

B. Group-theoretical background

We provide here an abstract description of the decomposition of the XMLD in a set of fundamental spectra. The analytical expressions for the angular dependence in a crystal field of tetragonal and octahedral point-group symmetry that are given in Secs. III C and III D are a special consequence of this, but can also be understood without going into the group theory.

The XMLD signal can be represented by a sum over multipole tensors,[41,42] where in the case of valence d electrons, orbital tensors up to rank 4 influence the spectral shape.[43] However, angular momentum conservation in the photon absorption process restricts the rank of the multipole tensors in the angular-dependent measurement.[44] The angular dependence of the XMLD spectrum due to rotation of a vector, such as the polarization vector of the light or the magnetization direction, can be described by a tensor of rank $k=2$, i.e., a quadrupole tensor with $2k+1=5$ components. The higher-order angular dependence can be measured using electric-quadrupole radiation, which, however, has a very low cross section in the soft x-ray region, and for this reason will be neglected. In the following we discuss the angular dependence of the XMLD in the point-group symmetry[45] of the absorbing atom, which is justified since the x-ray absorption process from a core level is localized around a single atomic site. While the magnetization has long-range order, it is the local magnetic moment that is measured in XMLD.

In spherical symmetry and in cubic crystal field symmetry there is no quadrupole moment and no magnetization direction, hence there is no XMLD. Breaking the spherical symmetry along an arbitrary direction by a magnetic field gives a distinct quantization axis, which allows one component of the quadrupole moment to be nonzero. (This component corresponds to the total symmetric representation 0 in SO_2 symmetry.) This results in one fundamental spectrum for the XMLD. As one is free to choose the direction of the quantization axis, the XMLD does not depend on the magnetization direction, and rotating the coordinate frame does not change the fundamental spectrum.

In the case of a cubic crystal field, distinctly different measurements can be taken along the fourfold and the threefold symmetry axes, which gives nonzero components of the quadrupole moment corresponding to the irreducible representations E and T_2, respectively. In D_4 crystal field symmetry there are four different irreducible representations: E (cubic) splits into A_1 and B_1, and T_2 (cubic) splits into E and B_2. Each representation has a corresponding fundamental spectrum.

The XMLD spectrum measured in arbitrary geometry can be written as a linear combination of the fundamental spectra,

$$I_{\mathrm{XMLD}}(h\nu,\phi,\theta) = \sum_n a_n(\phi,\theta) I_n(h\nu), \qquad (2)$$

where the angular and energy dependence is contained in the angular coefficients $a_n(\phi,\theta)$ and the fundamental spectra $I_n(h\nu)$, respectively. n is the number of fundamental spectra of the XMLD, which depends on the symmetry of the crystal, i.e., 1, 2, and 4 for SO_2, O_h, and D_4 symmetry, respectively. The angular dependence is furthermore dependent on the specific measurement geometry. Expressions for various measurement geometries in cubic symmetry have been given in Ref. 11. The measurement geometries for the linear dichroism and magnetic dichroism, defined in Eqs. (1a) and (1b), respectively, are the same but with **E** and **H** interchanged. The angular dependence for LD and MD is in this case the same. [We will use the subscript XMLD if we do

not make an explicit distinction between LD and MD, such as in Eq. (2).] However, the spectral shape of the fundamental spectra is not necessarily the same for LD and MD (see, Sec. III E). Also, the shape of the fundamental spectra sensitively depends on the electronic structure and composition of the material as well as on external factors such as temperature. These spectra can be calculated using a suitable model such as band-structure theory for itinerant systems or multiplet theory for localized materials (see, Sec. IV).

C. Tetragonal crystal field

We give here expressions for the case of D_4 crystal field symmetry, where the fourfold axis is along the z axis, which lies in the plane of orientation. Thus this allows us to use any plane of orientation that contains the [100] axis. The geometry is defined in Sec. III A and shown in Fig. 2.

We will start by assuming that the sample magnetization is saturated, i.e., that its direction is parallel to the applied field. The noncollinear case will be treated in Sec. III G. The angular dependence of the linear dichroism and magnetic dichroism, as defined by Eqs. (1a) and (1b), respectively, is the same, and is given by

$$I_{\mathrm{XMLD}}(\phi,\theta) = \frac{1}{4}[I_0 + 2I_{45} + I_{90}(\theta)] + \frac{1}{2}[I_0 - I_{90}(\theta)]\cos 2\phi$$
$$+ \frac{1}{4}[I_0 - 2I_{45} + I_{90}(\theta)]\cos 4\phi, \qquad (3)$$

which resembles Eq. (10) for the (011) plane in Ref. 11.

The I_0, I_{45}, and $I_{90}(\theta)$ are defined as the XMLD spectra for $\phi=0°$, $45°$, and $90°$, respectively. Due to the D_4 symmetry condition, $x=y \neq z$, the I_0 and I_{45} spectra are independent of θ. It then remains to know the azimuthal dependence in Eq. (3), which is given by

$$I_{90}(\theta) = \frac{1}{4}[3I_{90}^{\theta=0} + I_{45}^{xy} + (I_{90}^{\theta=0} - I_{45}^{xy})\cos 4\theta]. \qquad (4)$$

This equates for the (001) and (011) planes to $I_{90}(0)=I_{90}^{\theta=0}$ and $I_{90}(45)=\frac{1}{2}(I_{90}^{\theta=0}+I_{45}^{xy})$, respectively, where we define

$$I_{45}^{xy} \equiv I_{\mathrm{XA}}(\mathbf{E}_{90,45},\mathbf{H}_{90,45}) - I_{\mathrm{XA}}(\mathbf{E}_{90,45},\mathbf{H}_{90,135}). \qquad (5)$$

Thus, while I_{45} is the XMLD with $\phi=45°$ in the plane of orientation, I_{45}^{xy} is the corresponding XMLD in the xy plane. Note that I_{45} belongs to the twofold-degenerate representation containing I_{45}^{yz} and I_{45}^{zx}. To pick up the connection to group theory, the fundamental spectra I_0, $I_{90}^{\theta=0}$, I_{45}, and I_{45}^{xy} correspond to the representations A_1, B_1, E, and B_2, respectively, of the D_4 symmetry group.

D. Octahedral crystal field

The case of cubic symmetry can be directly derived from that of D_4, with Eq. (3) being equally applicable. Taking the three coordinate axes equivalent means that $I_{90}^{\theta=0}=I_0$ and $I_{45}^{xy}=I_{45}$, which simplifies Eq. (4) to

$$I_{90}(\theta) = \frac{1}{4}[3I_0 + I_{45} + (I_0 - I_{45})\cos 4\theta], \tag{6}$$

which for the (001) and (011) plane gives $I_{90}(0) = I_0$ and $I_{90}(45) = \frac{1}{2}(I_0 + I_{45})$, respectively. This confirms that for cubic symmetry there are only two fundamental spectra I_0 and I_{45}, which correspond to the representations E and T_2, respectively, of the octahedral symmetry groups (e.g., O, O_h, T, T_d).

The angular dependence of the XMLD in cubic symmetry can be elegantly rewritten as

$$I_{\mathrm{XMLD}}(\phi, \theta) = [1 - a(\phi, \theta)]I_0 + a(\phi, \theta)I_{45}, \tag{7}$$

where the angular-dependent coefficient $a(\phi, \theta)$ obtains the forms

$$a(\phi, 45) = \frac{1}{2}(3\cos 2\phi + 4)\sin^2 \phi, \tag{8a}$$

$$a(\phi, 0) = \frac{1}{2}(1 - \cos 4\phi) \tag{8b}$$

for the (011) and (001) planes, respectively.

This different way of presenting the results previously reported in Ref. 11 makes it more obvious that in the case of a known plane of orientation we can use the single parameter $a(\phi, \theta)$ to fit the experimental spectra. The goniometric functions in Eq. (8) restrict the parameter range to $0 \leqslant a(\phi, 45) \leqslant 1.021$ and $0 \leqslant a(\phi, 0) \leqslant 1$. Thus the coefficients of the I_0 and I_{45} terms in Eq. (7) are always positive, with the exception that $[1 - a(\phi, 45)]$ is only slightly negative near $\phi = 49.8°$. The benefit of this restricted parameter range for fitting the experimental spectra will be discussed in more detail in Sec. V A.

Note furthermore that for the [111] direction, where ϕ is at the magic angle in the $(01\bar{1})$ plane, Eq. (8a) gives $a(54.7, 45) = 1$, so that $I_{\mathrm{XMLD}}(54.7, 45) = I_{45}$, which thus gives the same spectrum as $I_{\mathrm{XMLD}}(45, 0)$.

E. Comparison between linear and magnetic dichroism

No distinction was made in Secs. III C and III D between rotation of **E** or **H**. Indeed, Eqs. (3)–(8) are valid in both cases. However, in D_4 symmetry the fundamental spectra have generally a different shape for rotation of **E** and **H**.

In systems that are noncubic the dichroism can have contributions from both the charge and magnetic anisotropy, so that rotation of **H** and **E** will lead to different results, which inevitably means that extra fundamental spectra are needed to describe this difference. However, the LD and MD spectra are not completely independent of each other. It can be shown that for D_4 symmetry, taking the fourfold axis along the z axis, the difference between the linear dichroism and magnetic dichroism, obtained by rotating **E** and **H**, respectively, results in

$$I_{\mathrm{LD}}(\phi, \theta) - I_{\mathrm{MD}}(\phi, \theta) = (I_0^{\mathrm{LD}} - I_0^{\mathrm{MD}})\cos 2\phi, \tag{9}$$

where the right-hand side is independent of θ. If the linear dichroism contains contributions from both magnetic and
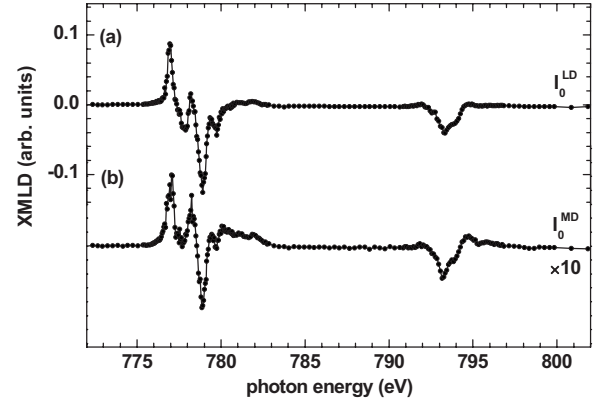

FIG. 3. Experimental Co $L_{2,3}$ XMLD spectra I_0 for CoFe$_2$O$_4$/SrTiO$_3$(011) obtained at $T = 420$ K and $H = 0.55$ T. Rotation of (a) the light polarization $I_0^{\mathrm{LD}} = I_{\mathrm{XA}}(\mathbf{E}_0, \mathbf{H}_0) - I_{\mathrm{XA}}(\mathbf{E}_{90}, \mathbf{H}_0)$, and (b) the magnetization $I_0^{\mathrm{MD}} = I_{\mathrm{XA}}(\mathbf{E}_0, \mathbf{H}_0) - I_{\mathrm{XA}}(\mathbf{E}_0, \mathbf{H}_{90})$. The strong reduction in the intensity for rotation of **H** is due to the incomplete magnetization saturation [see Eq. (12)].

charge anisotropy then $I_0^{\mathrm{LD}} \neq I_0^{\mathrm{MD}}$. The consequence of Eq. (9) is that only one extra spectrum, i.e., $I_0^{\mathrm{LD}} - I_0^{\mathrm{MD}}$, is needed to obtain the angular dependence of the magnetic dichroism from that of the linear dichroism (or vice versa). It also follows from Eq. (9) that

$$I_{45}^{\mathrm{LD}} = I_{45}^{\mathrm{MD}} \tag{10}$$

and

$$I_0^{\mathrm{LD}} + I_{90}^{\mathrm{LD}} = I_0^{\mathrm{MD}} + I_{90}^{\mathrm{MD}}$$
$$= I_{\mathrm{XA}}(\mathbf{E}_0, \mathbf{H}_0) + I_{\mathrm{XA}}(\mathbf{E}_{90}, \mathbf{H}_{90}) - I_{\mathrm{XA}}(\mathbf{E}_{90}, \mathbf{H}_0)$$
$$- I_{\mathrm{XA}}(\mathbf{E}_0, \mathbf{H}_{90}) \tag{11}$$

for any θ.

In the case of cubic symmetry, $I_{\mathrm{XA}}(\mathbf{E}_{0,0}, \mathbf{H}_{90,0}) = I_{\mathrm{XA}}(\mathbf{E}_{90,0}, \mathbf{H}_{0,0})$, so that rotation of either **E** or **H** from the [100] to the [010] direction results in the same XMLD, i.e., $I_0^{\mathrm{LD}} = I_0^{\mathrm{MD}}$. Substitution of this relation into Eq. (9) gives $I_{\mathrm{LD}}(\phi, \theta) = I_{\mathrm{MD}}(\phi, \theta)$. Thus in cubic symmetry the fundamental spectra are the same for linear and magnetic dichroism. The reason for this is clear: since there is no charge quadrupole moment in cubic symmetry, the linear dichroism is entirely due to the magnetic dichroism.

Comparison of the XMLD for rotation of **E** and **H** allows us to assess the influence of the charge anisotropy due to noncubic symmetry. Rotation of **H** does not probe the charge anisotropy, since the orbitals are fixed to the lattice. Rotation of **E** probes both the charge anisotropy and the magnetic anisotropy. Figure 3 shows the experimental Co $L_{2,3}$ XMLD spectra I_0^{LD} and I_0^{MD} for CoFe$_2$O$_4$/SrTiO$_3$(011) measured at $T = 420$ K and $H = 0.55$ T. For rotation of **H** the signal is reduced by about an order of magnitude due to the incomplete magnetization saturation (see, Sec. III G). For **H** at 90° (along the hard $[01\bar{1}]$ direction) the sample magnetization makes an angle $\tau \approx 20°$ with the [100] direction. There is a small difference in the line structure between the normalized I_0^{LD} and I_0^{MD} spectra, which reveals the presence of charge

anisotropy; however the cubic model should still be a reasonable approximation.

F. Relation to the magnetic anisotropy

The XMLD is of second order in the magnetization. Hence, in cubic symmetry the anisotropic XMLD would not directly measure the magnetocrystalline anisotropy, which in a cubic crystal is of fourth (and higher) order in the magnetization.[46] Also, since the $3d$ orbitals are fixed to the lattice, the charge quadrupole moment and the anisotropic spin-orbit interaction vanish in cubic symmetry. In lower than cubic symmetry these LS-coupled tensors give a contribution to the integrated XMLD intensities of the L_3 and L_2 edges, which can be related by sum rules to the ground-state expectation values of these tensors.[6,7] However, the integrated intensities are usually very small, and much harder to measure than the huge changes in positive and negative peak structures. These derivativelike spectral structures of the XMLD primarily originate from the spin and orbital moments, as has been shown by moment analysis.[43]

The anisotropy in the XMLD disappears when the crystal field interaction is set to zero, as discussed in Sec. III B. However, with a crystal field this anisotropy remains in the absence of $3d$ spin-orbit interaction. A similar observation was made by Kuneš and Oppeneer[13] for itinerant $3d$ metals. While this effect was dubbed "huge magnetocrystalline anisotropy of the XMLD,"[13,47] it would be more appropriate to refer to this phenomenon as a huge magneto-optical anisotropy.

Although so far no quantitative analysis has been attempted, it would be surprising if the magnetocrystalline anisotropy energy (MAE), which is of the order of a few μeV/atom in metallic systems, is the origin of the large anisotropy in the XMLD. Recent measurements by Kuch *et al.*[47] showed that a Co thin film with low MAE gives very similar XMLD line shapes as observed for Co thin films with high MAE.[7] While going from itinerant to localized materials the magnitude of the XMLD increases, measurements show that the anisotropy in the XMLD has a similar size in CoFe$_2$O$_4$ as in Fe$_3$O$_4$ (Ref. [11]) and NiFe$_2$O$_4$,[12] despite the fact that the MAE is much larger in CoFe$_2$O$_4$. These observations clearly indicate that the magnetocrystalline anisotropy is not the determining factor for the anisotropy in the XMLD, which instead arises due to geometrical effects, where the anisotropy in the XMLD scales with the strength of the crystal field. A larger crystal field distortion results in a larger change among the fundamental spectra. An average size crystal field (~ 1 eV) in $3d$ transition metal oxides gives changes in the anisotropy on the order of the XMLD spectrum itself.

G. Nonsaturated magnetization

For application to systems with strong magnetic anisotropy it is necessary to discuss the robustness of the measured fundamental spectra for incomplete magnetization saturation. While the angle between the applied field **H** and [100] is ϕ, in a nonsaturating field the angle between sample magnetization **M** and [100] will be $\tau \neq \phi$. The angle $|\phi - \tau|$ between **M** and **H** increases from zero to a maximum value when **H** rotates from an easy to a hard direction. Furthermore, $|\phi - \tau|$ decreases with increasing magnetization and goes to zero for a saturating field. The XMLD for **M** at the angle τ will be a different linear combination of fundamental spectra than at the angle ϕ, so that the spectral shape of the XMLD changes when the magnetization is reduced from saturation. For the measurements in the $(01\bar{1})$ plane (i.e., $\theta = 45°$) with the easy axis along [100] the $I_{MD}(\phi)$ can be written as

$$I_{MD}(0) = I(\mathbf{E}_0, \mathbf{M}_0) - I(\mathbf{E}_0, \mathbf{M}_\tau) = I_0 \sin^2 \tau, \quad (12a)$$

$$I_{MD}(90) = I(\mathbf{E}_{90}, \mathbf{M}_\tau - I(\mathbf{E}_{90}, \mathbf{M}_{180}) = I_{90} \sin^2 \tau, \quad (12b)$$

$$I_{MD}(45) = I(\mathbf{E}_{45}, \mathbf{M}_\tau) - I(\mathbf{E}_{45}, \mathbf{M}_{180-\tau}) = I_{45} \sin 2\tau, \quad (12c)$$

where τ in Eqs. (12a) and (12b) is the angle of **M** when **H** is along $\phi = 90°$ and τ in Eq. (12c) is the angle of **M** when **H** is along $\phi = 45°$.

Equation (12) shows that, for a nonsaturated sample magnetization, the XMLD spectra measured with **H** along $\phi = 0°$, 45°, and 90° correspond to the respective fundamental spectra I_0, I_{45}, and $I_{90}^{\theta = 45}$, multiplied by a magnetization-dependent scaling factor. This important result allows us to obtain the anisotropic XMLD also for samples with very large anisotropy, such as the Co oxides. It demonstrates that in this particular geometry the degree of sample magnetization does not influence the shape of the fundamental spectra. The simple angular dependencies in Eq. (12) arise because **E** is along a principal axis; therefore these expressions do not apply when the sample has an arbitrary crystalline orientation.

IV. CALCULATIONS

A. Multiplet structure

Figure 4 shows the theoretical spectra using atomic multiplet calculations following the method described in Ref. [5]. The $L_{2,3}$ XA spectra with **H** and **E** along specified directions were obtained from the electric-dipole-allowed transitions between the ground-state $3d^7$ and the final-state $2p^5 3d^8$ configurations. The wave functions of ground and final states were calculated in intermediate coupling using Cowan's Hartree-Fock code with relativistic correction.[48] The Slater and spin-orbit parameters are as tabulated in Ref. [49]. Interatomic screening and mixing was taken into account by reducing the atomic values of the Slater integrals $F^k(3d,3d)$, $F^k(2p,3d)$, and $G^k(2p,3d)$ to 70%, 80%, and 65%, respectively. For the octahedral site a crystal field of $10Dq = 0.9$ eV and an exchange field of $g\mu_B H = 12.6$ meV were used. (The value for the exchange interaction has been taken from neutron scattering measurements on CoO.[50,51]) The calculated results were broadened by a Lorentzian of $\Gamma = 0.1$ (0.3) eV for the L_3 (L_2) edge to account for intrinsic linewidth broadening and a Gaussian of $\sigma = 0.2$ eV for the instrumental broadening.

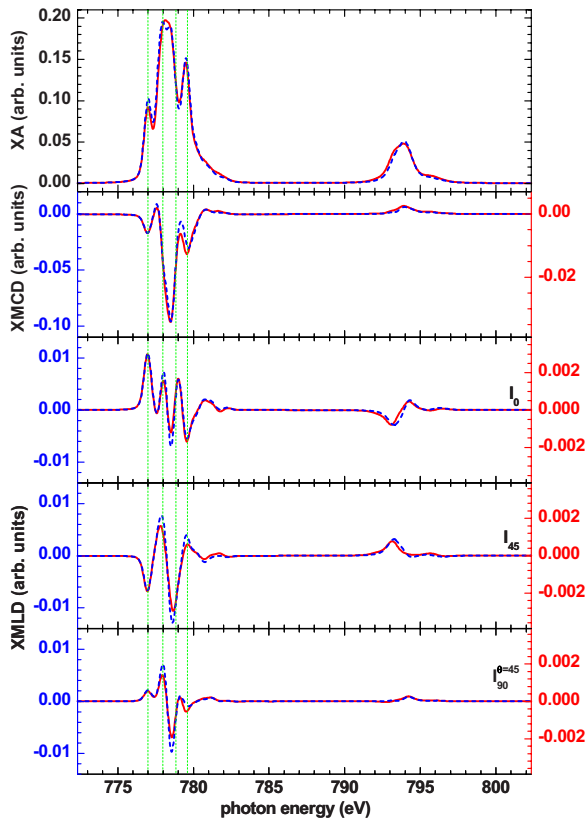In Fig. 1 we compare the theoretical spectra (red curves) from Fig. 4 for 0 K with the experimental spectra (black

FIG. 4. (Color online) Theoretical XA, XMCD, and XMLD (I_0, I_{45}, and $I_{90}^{\theta=45}$) spectra at the $L_{2,3}$ edge for Co^{2+} in octahedral crystal field at a temperature of 0 K (blue dashed curves) and at room temperature (red solid curves), calculated using an atomic multiplet model for the transition $Co\ 3d^7 \rightarrow 2p^5 3d^8$, in octahedral crystal field of $10Dq=0.9$ eV. Note the different intensity scale of the dichroic spectra for each temperature.

dots). While the agreement between experiment and theory is good, an even better agreement would be obtained if the two middle peaks (at ∼778 and ∼779 eV) in the calculated L_3 spectrum were shifted by 0.4 eV compared to the rest of the spectrum; the same energy shift can be observed in all spectra (XA, XMCD, and XMLD). The origin of this shift might be a combination of crystal field distortion and configurational mixing. Apart from this there is a good agreement between the experiment and the calculation for the atomic d^7 configuration, where the crystal field $10Dq$ is the only essential parameter. The main disagreement is found for the feature at ∼780 eV, which is probably caused by mixing with the d^8 configuration.

There are of course many ways to improve these atomic calculations. We also performed calculations using a cluster model or Anderson impurity model with different $3d^n$ configurations.[52] For CoO, the ground state is expected to have 80% d^7, 19% d^8, and 1% d^9 character, so that the d count is 7.21. This, however, does not significantly modify the ground-state symmetry, nor the spectra. Since in the final state the Coulomb interaction of the core hole is efficiently screened by the extra d electron, the relative energy positions of the configurations in the initial and final states are about the same.[53] Consequently, there is no significant change in

the hybridization after $2p$ absorption, which explains the absence of a distinct charge-transfer satellite in XA spectra. Both the crystal field and the anisotropic hybridization (mixing) contribute to the $3d$ level splitting. The anisotropic mixing has a strong effect on the orbital to spin magnetic moment ratio, which can sensitively alter the $L_3 : L_2$ intensity ratio of the dichroism.

Tetragonal distortion of the cubic symmetry will induce spectral changes, with almost unlimited scope for fitting the experimental data.[8] Some examples are shown in Sec. V B. We found that within realistic variations of the parameters the peak positions and intensities do change to certain degree, but that the essential features, and especially the sign of the dichroism of the larger peaks, do not change very much. This allows us to transfer the results from $CoFe_2O_4$ to antiferromagnetic CoO, where the divalent Co is also nearly octahedrally surrounded by oxygen ligands, with similar crystal field strength and minor distortion.

B. Spin-orbit splitting and temperature dependence

It is interesting to consider the consequences of the $3d$ spin-orbit interaction for the Co^{2+} configuration and several previous calculations have already shown its effect on the $L_{2,3}$ absorption spectra.[5,8,26,52,54–59] The spectral shape depends on the Boltzmann population of the spin-orbit split levels in the ground state, which makes it important to investigate its influence on the anisotropic XMLD.

The d^7 configuration in O_h symmetry has a spin quintet ground state $t_{2g}^5 e_g^2$ ($^4T_{1g}$), which is split by first-order spin-orbit interaction into four levels E', U', U', and E'. The lowest level is E', with the first excited level U' at ∼50 meV higher energy. The magnetic exchange field in C_{4h} symmetry breaks the Kramers degeneracy. The E' splits into two magnetic sublevels with an energy separation of ∼H_{ex} and the U' splits into four magnetic sublevels. Since the first-order spin-orbit splitting (∼50 meV) is well above room temperature (RT) (RT corresponds to 26 meV), only the E' level is significantly Boltzmann populated. On the other hand, H_{ex} is of the order of RT, so that there will be a Boltzmann distribution over the two magnetic sublevels of E', giving rise to a strong temperature dependence. However, the shape of the dichroism spectra of the two conjugate states is quite similar but with opposite sign, so that the overall shape of the Boltzmann-summed spectrum does not change much with temperature, but shows a gradual reduction in magnitude with increasing temperature. In order to illustrate this, Fig. 4 compares the calculated spectra for 0 K (blue dashed curves) and at RT (red solid curves), where we draw attention to the different intensity scales of the dichroism spectra for the two different temperatures. It is clear that none of the peak structures is actually changing sign. More pronounced temperature effects can occur when the cubic symmetry is strongly distorted.

V. APPLICATION

As mentioned in the Introduction, an important application of the anisotropic XMLD is the determination of the

spin-axis orientation in thin films and multilayers. Confronted with an unknown orientation of the magnetic domain structure of a divalent Co oxide film, the relative intensities in the fourfold peak structure of the Co L_3 XA offer a very sensitive tool to determine the spin-axis orientation with respect to the crystalline axes. In the case of samples with domain structure, such a study can be performed using photoemission electron microscopy (PEEM) by rotating the linear polarization, as was recently demonstrated by Czekaj *et al.*[14] in a study on LaFeO$_3$. For the PEEM experiment, the sample has to be at remanence, and the XA is measured by rotating **E**. The strongly anisotropic XMLD will give for the different domains a clear contrast in the XA using linearly polarized light at fixed photon energy. However, until now it has been unclear how to analyze the data, since the anisotropic XMLD spectra were not available in the literature.

A. Cubic symmetry

Cubic systems have the important advantage that the magnetic anisotropy can be accurately studied with PEEM by rotating **E**, since it gives the same result as rotating **H**. Within the formalism for cubic symmetry, Eqs. (6)–(8) should allow a unique fit to the rich structure in the L_3 XMLD, from which the coefficient $a(\phi, \theta)$ can be determined. However, a particular solution for the angular parameter can correspond to several possible orientations of the spin axis. This is perhaps most remarkably illustrated by the fact that the I_{45} spectrum corresponds to both $I(\phi = 45°, \theta = 0°)$ and $I(\phi = 54.7°, \theta = 45°)$. Additional information, such as knowledge of the orientation of the crystalline axes and/or the crystal plane, or measurements using different geometries, will help to obtain a unique determination of the spin axis.

As a practical example we will discuss the sensitivity of the XA spectral shape to the spin-axis orientation relative to the crystalline axes. Figure 5 shows the calculated spectra in cubic symmetry, where rotation of either **E** or **H** gives the same result. Here, we take **H** as the spin axis. (There is no external magnetic field.) Spectra with the spin axis along [100] are displayed in Fig. 5(a), which shows $I_{XA}(\mathbf{E}_0, \mathbf{H}_0)$ and $I_{XA}(\mathbf{E}_{90}, \mathbf{H}_0)$ together with their difference spectrum I_0. These spectra are independent of the angle θ, so that the rotation of **E** can be in an arbitrary plane of orientation. We will make reference to the four peaks centered around 777, 778.2, 778.9, and 779.7 eV, respectively, in the L_3 edge. It is seen that the first two of these peaks (i.e., those at the low-energy side) of the L_3 XA have a higher intensity for **E**‖**H** than for **E**⊥**H**, while the opposite is true for the last two peaks of the L_3 XA spectrum.

When the spin axis **H** is along ⟨110⟩, the XMLD can be measured by rotating **E** in either the (001) plane or the (011) plane, which leads to different results. The spectra for rotating **E** in the (001) plane (i.e., $\theta = 0°$) are displayed in Fig. 5(b), which shows $I_{XA}(\mathbf{E}_{45}, \mathbf{H}_{45})$ and $I_{XA}(\mathbf{E}_{135}, \mathbf{H}_{45})$ together with their difference spectrum I_{45}. While the second and fourth peaks in the L_3 XA have higher intensity for **E**‖**H**, the first and third peaks have higher intensity for **E**⊥**H**. The other situation, where the XMLD is measured by rotating **E**
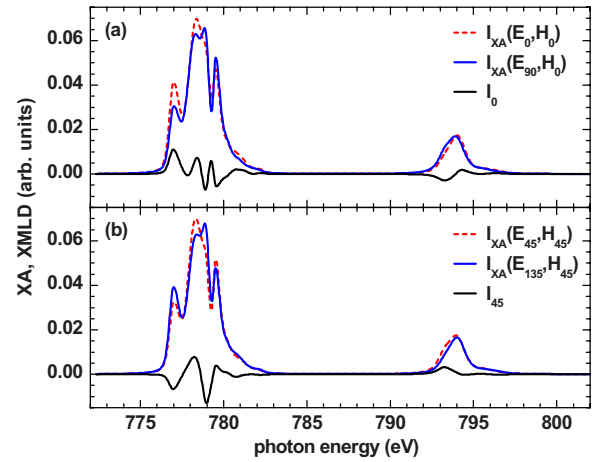

FIG. 5. (Color online) Calculated XA spectra in octahedral crystal field. (a) $I_{XA}(\mathbf{E}_0, \mathbf{H}_0)$ (dashed red line), i.e., **E**‖**H**‖[100], and $I_{XA}(\mathbf{E}_{90}, \mathbf{H}_0)$ [solid blue (gray) line], i.e., **E**⊥**H**‖[100], together with their difference spectrum I_0 (solid black line). The rotation of **E** can be in any plane-of-orientation containing [100]. (b) $I_{XA}(\mathbf{E}_{45}, \mathbf{H}_{45})$ (dashed red line), i.e., **E**‖**H**‖[110], and $I_{XA}(\mathbf{E}_{135}, \mathbf{H}_{45})$ [solid blue (gray) line], i.e., **E**‖[$\bar{1}$10] and **H**‖[110], together with their difference spectrum I_{45} (solid black line). Hence, the rotation of **E** is here in the (001) plane.

in the (011) plane, corresponds to the spectra $I_{XA}(\mathbf{E}_{90}, \mathbf{H}_{90})$ and $I_{XA}(\mathbf{E}_{180}, \mathbf{H}_{90})$ with $\theta = 45°$. The difference spectrum $I_{90}^{\theta=45}$ is shown in Fig. 1, from which it is clear that for **E**‖**H** the second peak in the L_3 XA has higher intensity and the third peak has lower intensity than for **E**⊥**H**. This is the same as when **E** is rotated in the (001) plane. However, for rotation in the (011) plane, for the first peak in the L_3 as well as the entire L_2 edge, the intensity remains about the same, while it changes for rotation in the (001) plane. Therefore, while the spin axes along ⟨100⟩ and ⟨110⟩ give characteristic differences in the XA spectra, it is important to take into account the geometry of the measurement.

B. Tetragonal symmetry

Strained CoO thin films can exhibit a large magnetocrystalline anisotropy, which will require the formalism of tetragonally distorted symmetry as described in Sec. III C. The fundamental spectra can be readily calculated in D_4 symmetry using multiplet theory with crystal field parameters Dq, Ds, and Dt.[60] Fortunately, cubic symmetry remains often a good approximation, e.g., within the accuracy of the measurement there are only two fundamental spectra for nearly cubic systems such as Fe$_3$O$_4$ (Ref. 11) and NiO.[12] The relation $I_{90}^{\theta=45} = \frac{1}{2}(I_0 + I_{45})$ provides a check on cubic symmetry [see remark below Eq. (6)], which is nicely confirmed by our experimental data in the case of CoFe$_2$O$_4$(011), as shown in Fig. 1 (bottom panel). On the other hand, some distortion from cubic symmetry must be present as evidenced by the fact that I_0^{LD} and I_0^{MD} in Fig. 3 do not have exactly the same spectral shape.

It is interesting to see how the magnetic dichroism and linear dichroism can become quite different for a tetragonal
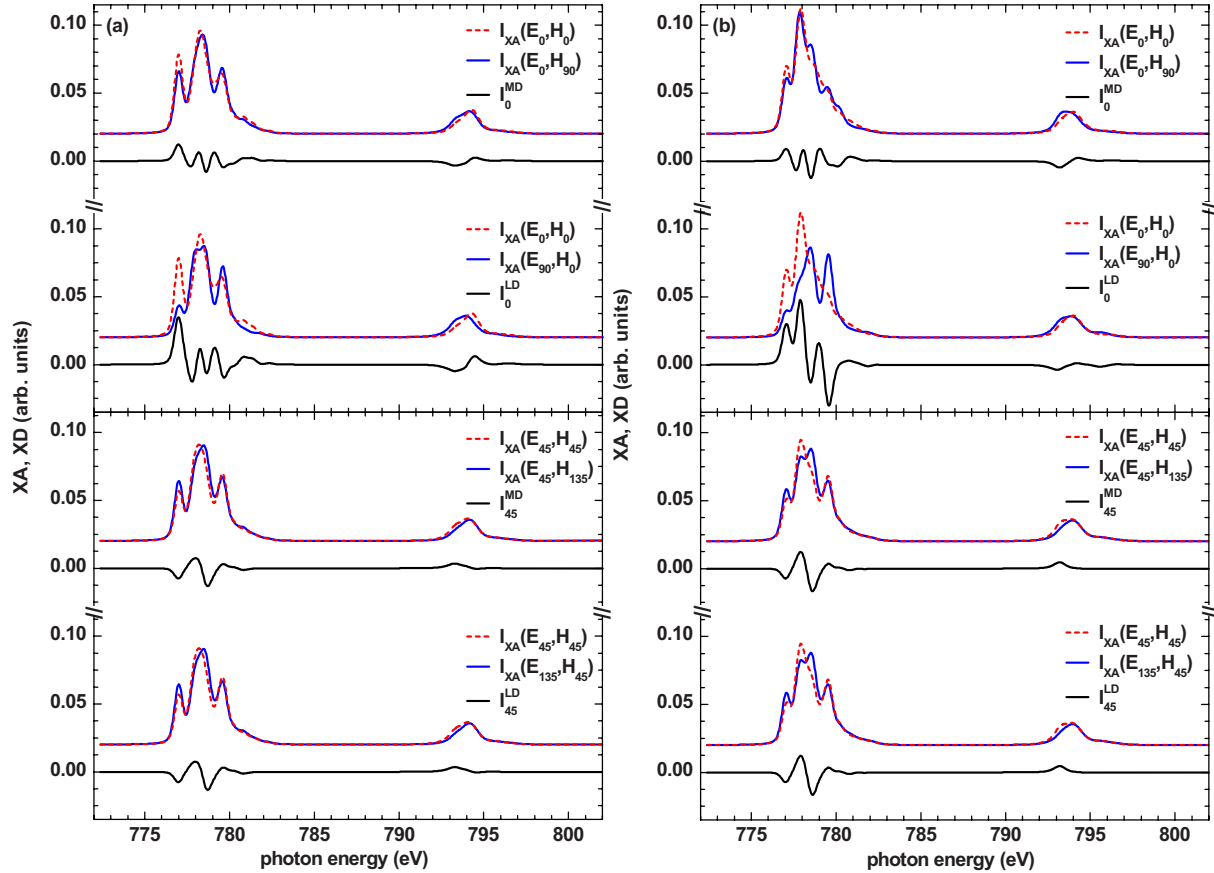
FIG. 6. (Color online) Calculated XA spectra for D_4 crystal field showing the difference for magnetic dichroism and linear dichroism. Two different distortions are shown with parameter sets (a) $10Dq=0.9$, $Ds=-0.04$, $Dt=-0.013$ and (b) $10Dq=1.06$, $Ds=0.013$, $Dt =0.032$ (all in eV). Upper two panels: $I_{XA}(\mathbf{E}_0,\mathbf{H}_0)$ (dashed red line) with either $I_{XA}(\mathbf{E}_0,\mathbf{H}_{90})$ or $I_{XA}(\mathbf{E}_{90},\mathbf{H}_0)$ [solid blue (gray) lines] together with the difference spectra I_0^{MD} or I_0^{LD} (solid black lines), respectively. Lower two panels: $I_{XA}(\mathbf{E}_{45},\mathbf{H}_{45})$ (dashed red line) with either $I_{XA}(\mathbf{E}_{45},\mathbf{H}_{135})$ or $I_{XA}(\mathbf{E}_{135},\mathbf{H}_{45})$ [solid blue (gray) lines], together with the difference spectra I_{45}^{MD} or I_{45}^{LD} (solid black lines), respectively. Note that while I_0^{LD} is strongly different for the two distortions, I_0^{MD} has practically the same shape as for O_h symmetry. I_{45}^{MD} and I_{45}^{LD} are the same, and very similar as for O_h symmetry (cf Fig. 5).

distortion. As an example, Fig. 6 shows the calculated XA spectra in D_4 crystal field symmetry for two different distortions with parameter sets (a) $10Dq=0.9$, $Ds=-0.04$, $Dt= -0.013$ and (b) $10Dq=1.06$, $Ds=0.013$, $Dt=0.032$ (all in eV). Case (a) resembles epitaxial CoO/MnO(100) of Ref. 8 and case (b) represents a deliberately large chosen distortion to test the validity of the cubic approach. As can be verified from the figure, the I_0^{LD} spectrum is strongly dependent on the distortion, since it changes the charge anisotropy. On the other hand, the spectral shape of the I_0^{MD} spectrum is practically independent of the distortion and very similar as for O_h symmetry (see Fig. 5). Furthermore, the I_{45}^{MD} and I_{45}^{LD} spectra are the same and likewise very similar as for O_h symmetry, which demonstrates the validity of Eq. (10). We can conclude that under the distortion the magnetic dichroism remains a reliable indicator for the spin axis, while the linear dichroism may become unreliable for this task. Thus these calculations for distorted symmetry confirm the transferrability of the magnetic dichroism from CoFe$_2$O$_4$ to other Co^{2+} compounds with might have different crystal fields, such as CoO.

We can also compare our results with the recent XA measurements by Csiszar *et al.*[8] on CoO/MnO(100) and

CoO/Ag(100), where the antiferromagnetic spin axis is perpendicular and in plane, respectively. Unfortunately, these authors have not specified unambiguously the orientation of moments and polarization relative to the crystal lattice, while the angle to the surface normal is noted, the in-plane angle is not. The spectra for CoO/MnO(100) with different directions of **E** (Fig. 2 in Ref. 8) can be compared directly with our results in Fig. 6(a). Our results show that the linear dichroism leads to changes in the individual peaks in a similar—but much stronger—way as for the magnetic dichroism. In particular, the change in the leading peak (~777 eV) can be ascribed mainly to charge anisotropy instead of magnetic anisotropy. This clearly illustrates the danger that exists in measuring the XMLD by rotating **E**. If the charge anisotropy were of opposite site sign, the wrong sign of the magnetic anisotropy might be concluded.

C. L_2 edge spectra

In contrast with the Co^{2+} L_3 edge, the L_2 edge does not allow an unambiguous determination of the spin axis with respect to the crystal axes. This has recently been demon-

strated for the case of the Ni^{2+} L_2 edge, where the same effect occurs,[12] although this effect is not general for the $3d$ transition metal L_2 edges.[11] As seen from e.g., Fig. 1, the two fundamental spectra at the Co^{2+} L_2 edge have very similar shape but are opposite in sign, i.e., $I_{45} \approx -I_0$. Consequently, the L_2 XMLD signal practically disappears for $I_{90}^{\theta=45} = \frac{1}{2}(I_0 + I_{45})$, as can be verified from Fig. 1. Therefore, a fit would not be able to distinguish between I_0 and I_{45}, so that the angular dependence provides only limited information. Although the shape of the L_2 XMLD does not change, the sign of the spectrum can still give us a possible range for the value of ϕ, as follows. Substituting $I_{45} = -I_0$ into Eq. (7) gives $I_{XMLD}(\phi, \theta) = [1 - 2a(\phi, \theta)]I_0$, where $[1 - 2a(\phi, \theta)]$ is positive in the first quadrant for $0° < \phi < 24.1°$ in the (011) plane and for $0° < \phi < 22.5°$ and $67.5° < \phi < 90°$ in the (001) plane, while negative elsewhere. Therefore, analysis of the L_2 edge can still provide support for any assignment extracted from the L_3 edge structure.

Thus, to find the spin axis one should employ the L_3 edge which not only shows characteristically different spectral shapes for I_0 and I_{45}, but also offers a richer and more intense signal. Although, such a recommendation might sound trivial, almost all studies performed so far on NiO have used only the L_2 edge, as was put straight recently in Ref. 12.

VI. CONCLUSIONS

We have presented a group-theoretical approach in order to explain the influence of the crystal field on the anisotropic XMLD. In a cubic crystal field, the XMLD can be written as a linear combination of two fundamental spectra I_0 and I_{45}, with distinctly different spectral shapes. However, the shape is the same for rotation of either the linear light polarization **E** or the magnetization direction **H**. In contrast, in tetragonal crystal field symmetry, the XMLD is a linear combination of four fundamental spectra, with different shapes for rotation of either **E** or **H**. However, these differences require only one additional spectrum. The difference in the fundamental spectra for linear dichroism (i.e., rotation of **E**) and magnetic dichroism (i.e., rotation of **H**) allows us to assess the influence of the charge anisotropy by a noncubic distortion. We have shown that the anisotropy in the spectral shape of the XMLD depends on the strength of the crystal field, and that there is no evidence that it relates to the magnetocrystalline anisotropy energy. The anisotropic XMLD does not vanish when the spin-orbit interaction is zero. According to the sum rules the magnetocrystalline anisotropy energy affects only the integrated intensity of the $L_3 : L_2$ branching ratio.

We measured the anisotropic XMLD at the Co $L_{2,3}$ edges of $CoFe_2O_4(011)$ and compared the results to theoretical spectra for Co^{2+}. The observed anisotropy in XMLD was shown to be in good agreement with atomic multiplet calculations in cubic crystal field. The comparison of our results for $CoFe_2O_4$ to results reported for CoO indicates that the fundamental spectra exhibit similar spectral shapes for ferromagnet and antiferromagnet. This is useful since in a ferro- or ferrimagnet the fundamental spectra can be measured more easily and the results can then be transferred to an antiferromagnet where the moments are not so easily rearranged. We also demonstrated that the fundamental spectra could be measured even though the sample was actually not magnetically saturated.

While the rich structure in the Co^{2+} L_3 XMLD provides a sensitive probe to determine the orientation of the spin axis in Co oxides, at the L_2 edge the information obtained from the anisotropic XMLD is limited, since the two fundamental spectra have almost the same spectral shape but with opposite sign.

The method of decomposing the XMLD in fundamental spectra, as presented in this paper, is generally applicable, and can be used for other $3d$ transition metal systems as well. It provides a powerful tool to analyze the angular dependence of the x ray absorption and to obtain from it the orientation of the spin axis with respect to the crystallographic axes. Cubic systems offer the important advantage that the magnetic anisotropy can be studied with PEEM simply by rotating **E**. With caution, noncubic systems can also be studied by rotating **E**, as is the preferred method in PEEM. However, we have emphasized the complications in the linear dichroism arising from the charge anisotropy when the cubic symmetry is strongly distorted. On the other hand, the magnetic dichroism remains largely unaffected by the symmetry distortion.

---

*Also at School of Earth, Atmospheric and Environmental Sciences, University of Manchester, Manchester M13 9PL, United Kingdom.

†Also at School of Applied Physics, Cornell University, Ithaca, NY 14853.

[1] W. H. Meiklejohn and C. P. Bean, Phys. Rev. **102**, 1413 (1956).

[2] B. Dieny, V. S. Speriosu, S. S. P. Parkin, B. A. Gurney, D. R. Wilhoit, and D. Mauri, Phys. Rev. B **43**, 1297 (1991).

[3] J. Stohr, A. Scholl, T. J. Regan, S. Anders, J. Luning, M. R. Scheinfein, H. A. Padmore, and R. L. White, Phys. Rev. Lett. **83**, 1862 (1999).

[4] G. van der Laan, B. T. Thole, G. A. Sawatzky, J. B. Goedkoop, J. C. Fuggle, J.-M. Esteva, R. Karnatak, J. P. Remeika, and H. A. Dabkowska, Phys. Rev. B **34**, 6529 (1986).

[5] G. van der Laan and B. T. Thole, Phys. Rev. B **43**, 13401 (1991).

[6] G. van der Laan, Phys. Rev. Lett. **82**, 640 (1999).

[7] S. S. Dhesi, G. van der Laan, E. Dudzik, and A. B. Shick, Phys. Rev. Lett. **87**, 067201 (2001).

[8] S. I. Csiszar, M. W. Haverkort, Z. Hu, A. Tanaka, H. H. Hsieh, H.-J. Lin, C. T. Chen, T. Hibma, and L. H. Tjeng, Phys. Rev. Lett. **95**, 187205 (2005).

[9] P. Kuiper, B. G. Searle, L.-C. Duda, R. M. Wolf, and P. van der Zaag, J. Electron Spectrosc. Relat. Phenom. **86**, 107 (1997).

[10] A. A. Freeman, K. W. Edmonds, G. van der Laan, N. R. S. Farley, T. K. Johal, E. Arenholz, R. P. Campion, C. T. Foxon, and B. L. Gallagher, Phys. Rev. B **73**, 233303 (2006).

[11] E. Arenholz, G. van der Laan, R. V. Chopdekar, and Y. Suzuki, Phys. Rev. B **74**, 094407 (2006).

[12] E. Arenholz, G. van der Laan, R. V. Chopdekar, and Y. Suzuki, Phys. Rev. Lett. **98**, 197201 (2007).

[13] J. Kuneš and P. M. Oppeneer, Phys. Rev. B **67**, 024431 (2003).

[14] S. Czekaj, F. Nolting, L. J. Heyderman, P. R. Willmott, and G. van der Laan, Phys. Rev. B **73**, 020401 (2006).

[15] S. Maat, M. J. Carey, E. E. Fullerton, T. X. Le, P. M. Rice, and B. A. Gurney, Appl. Phys. Lett. **81**, 520 (2002).

[16] M. J. Carey, S. Maat, P. M. Rice, R. F. C. Farrow, R. F. Marks, A. Kellock, P. Nguyen, and B. A. Gurney, Appl. Phys. Lett. **81**, 1044 (2002).

[17] K. V. O'Donovan, J. A. Borchers, S. Maat, M. J. Carey, and B. A. Gurney, J. Appl. Phys. **95**, 7507 (2004).

[18] A. V. Ramos, J.-B. Moussy, M.-J. Guittet, M. Gautier-Soyer, C. Gatel, P. Bayle-Guillemaud, B. Warot-Fonrose, and E. Snoeck, Phys. Rev. B **75**, 224421 (2007).

[19] R. V. Chopdekar and Y. Suzuki, Appl. Phys. Lett. **89**, 182506 (2006).

[20] Y. Suzuki, G. Hu, R. B. van Dover, and R. J. Cava, J. Magn. Magn. Mater. **191**, 1 (1999).

[21] A. Lisfi and C. M. Williams, J. Appl. Phys. **93**, 8143 (2003).

[22] L. Horng, G. Chern, M. C. Chen, P. C. Kang, and D. S. Lee, J. Magn. Magn. Mater. **270**, 389 (2004).

[23] S. A. Chambers, R. F. C. Farrow, S. Maat, M. F. Toney, L. Folks, J. G. Catalano, T. P. Trainor, and J. G. E. Brown, J. Magn. Magn. Mater. **246**, 124 (2002).

[24] Z. Szotek, W. M. Temmerman, D. Kodderitzsch, A. Svane, L. Petit, and H. Winter, Phys. Rev. B **74**, 174431 (2006).

[25] J. R. Singer, Phys. Rev. **104**, 929 (1956).

[26] G. Ghiringhelli, L. H. Tjeng, A. Tanaka, O. Tjernberg, T. Mizokawa, J. L. de Boer, and N. B. Brookes, Phys. Rev. B **66**, 075101 (2002).

[27] J.-I. Hong, T. Leo, D. J. Smith, and A. E. Berkowitz, Phys. Rev. Lett. **96**, 117204 (2006).

[28] P. Miltenyi, M. Gierlings, J. Keller, B. Beschoten, G. Guntherodt, U. Nowak, and K. D. Usadel, Phys. Rev. Lett. **84**, 4224 (2000).

[29] K. Takano, R. H. Kodama, A. E. Berkowitz, W. Cao, and G. Thomas, Phys. Rev. Lett. **79**, 1130 (1997).

[30] P. J. van der Zaag, Y. Ijiri, J. A. Borchers, L. F. Feiner, R. M. Wolf, J. M. Gaines, R. W. Erwin, and M. A. Verheijen, Phys. Rev. Lett. **84**, 6102 (2000).

[31] F. Radu, M. Etzkorn, R. Siebrecht, T. Schmitte, K. Westerholt, and H. Zabel, Phys. Rev. B **67**, 134409 (2003).

[32] M. Gruyters, Europhys. Lett. **77**, 57006 (2007).

[33] P. Weinberger, Phys. Rev. B **75**, 064405 (2007).

[34] T. Blachowicz, A. Tillmanns, M. Fraune, R. Ghadimi, B. Beschoten, and G. Güntherodt, Phys. Rev. B **75**, 054425 (2007).

[35] Y. Suzuki, R. B. van Dover, E. M. Gyorgy, J. M. Phillips, V. Korenivski, C. H. C. D. J. Werder, R. J. Cava, J. J. Krajewski, J. W. F. Peck, and K. B. Do, Appl. Phys. Lett. **68**, 714 (1996).

[36] A. T. Young, E. Arenholz, S. Marks, R. Schlueter, C. Steier, H. A. Padmore, A. P. Hitchcock, and D. G. Castner, J. Synchrotron Radiat. **9**, 270 (2002).

[37] E. Arenholz and S. O. Prestemon, Rev. Sci. Instrum. **76**, 083908 (2005).

[38] F. Sette, C. T. Chen, Y. Ma, S. Modesti, and N. V. Smith, in *X-ray and Inner-Shell Processess*, edited by T. Carlson, M. O. Krause, and S. T. Manson, AIP Conf. Proc. No. 215 (AIP, New York, 1990), p. 787.

[39] L. Braicovich, G. Ghiringhelli, A. Tagliaferri, G. van der Laan, E. Annese, and N. B. Brookes, Phys. Rev. Lett. **95**, 267402 (2005).

[40] K. W. Edmonds, G. van der Laan, A. Freeman, N. R. S. Farley, T. K. Johal, R. P. Campion, C. T. Foxon, B. L. Gallagher, and E. Arenholz, Phys. Rev. Lett. **96**, 117207 (2006).

[41] P. Carra, H. König, B. T. Thole, and M. Altarelli, Physica B **192**, 182 (1993).

[42] J. Luo, G. T. Trammell, and J. P. Hannon, Phys. Rev. Lett. **71**, 287 (1993).

[43] G. van der Laan, Phys. Rev. B **55**, 8086 (1997).

[44] G. E. Steadman, Adv. Phys. **34**, 513 (1985).

[45] P. H. Butler, *Point Group Symmetry, Applications, Methods and Tables* (Plenum, New York, 1981).

[46] F. Brailsford, *Physical Principles of Magnetism* (Van Nostrand, London, 1966).

[47] W. Kuch, F. Offi, L. I. Chelaru, J. Wang, K. Fukumoto, M. Kotsugi, J. Kirschner, and J. Kunes, Phys. Rev. B **75**, 224406 (2007).

[48] R. D. Cowan, *The Theory of Atomic Structure and Spectra* (University of California Press, Berkeley, 1982).

[49] G. van der Laan and I. W. Kirkman, J. Phys.: Condens. Matter **4**, 4189 (1992).

[50] M. D. Rechtin and B. L. Averbach, Phys. Rev. B **5**, 2693 (1972).

[51] J. Sakurai, W. J. L. Buyers, R. A. Cowley, and G. Dolling, Phys. Rev. **167**, 510 (1968).

[52] L. Braicovich, A. Tagliaferri, G. van der Laan, G. Ghiringhelli, and N. B. Brookes, Phys. Rev. Lett. **90**, 117401 (2003).

[53] G. van der Laan, J. Zaanen, G. A. Sawatzky, R. Karnatak, and J.-M. Esteva, Phys. Rev. B **33**, 4253 (1986).

[54] K. Okada and A. Kotani, J. Phys. Soc. Jpn. **61**, 449 (1992).

[55] A. Tanaka and T. Jo, J. Phys. Soc. Jpn. **61**, 2040 (1992).

[56] S. Imada and T. Jo, J. Magn. Magn. Mater. **104-107**, 1992 (2001).

[57] T. Jo and T. Shishidou, J. Phys. Soc. Jpn. **67**, 2505 (1998).

[58] M. Magnuson, S. M. Butorin, J.-H. Guo, and J. Nordgren, Phys. Rev. B **65**, 205106 (2002).

[59] G. van der Laan, G. Ghiringhelli, A. Tagliaferri, N. B. Brookes, and L. Braicovich, Phys. Rev. B **69**, 104427 (2004).

[60] G. van der Laan, Lect. Notes Phys. **697**, 143 (2006).